Journal of King Saud University – Science (2015) 27, 209–216

King Saud University
Journal of King Saud University – Science
www.ksu.edu.sa
www.sciencedirect.com

ORIGINAL ARTICLE

Two-field-variable meshless method based on moving kriging interpolation for solving simply supported thin plates under various loads

S. Kaewumpai, A. Luadsong *

Department of Mathematics, Faculty of Science, King Mongkut's University of Technology Thonburi (KMUTT), Bangkok 10140, Thailand

Received 13 June 2014; accepted 8 December 2014
Available online 16 December 2014

KEYWORDS

Biharmonic equation;
Meshless method;
Moving kriging interpolation;
Thin plate bending problems

Abstract Meshless method choosing Heaviside step function as a test function for solving simply supported thin plates under various loads is presented in this paper. The shape functions using regular and irregular nodal distribution as well as order of polynomial basis choice are constructed by moving kriging interpolation. Alternatively, two-field-variable local weak forms are used in order to decompose the governing equation, biharmonic equation, into a couple of Poisson equations and then impose straightforward boundary conditions. Selected numerical examples are considered to examine the applicability, the easiness, and the accuracy of the proposed method. Comparing to an exact solution, this robust method gives significantly accurate numerical results, implementing by maximum relative error and root mean square relative error.

1. Introduction

The structures of plate are one of the important components in various applications. There are many scientists or researchers who have analyzed these structures. Exact analysis for such plates is usually very difficult, in spite of the existence of analytical solution in some special cases of geometry and loads. Therefore, various numerical methods have been developed. Meshless method has become very attractive and efficient for development of adaptive methods for solving thin plate bending problem. The main advantage of meshless methods is to get rid of or at least alleviate the difficulty of meshing and re-meshing the entire plate structure. For analysis of thin plate bending, it is well known that high order derivatives of field variables in the governing equation give rise to difficulties in solution of boundary value problems because of worse accuracy of numerically evaluated high order derivatives. The order of the differential operator can be decreased mathematically by decomposing this operator into two lower order differential operators with introducing new field variables.

To circumvent the problems associated with meshing, a number of works for plates have been investigated based on meshless methods. Krysl and Belytschko (1995) first employed the element free Galerkin method (EFGM) to analyze the thin

* Corresponding author.
E-mail address: anirut.lua@kmutt.ac.th (A. Luadsong).
Peer review under responsibility of King Saud University.

Production and hosting by Elsevier

http://dx.doi.org/10.1016/j.jksus.2014.12.003

plate problems while Liu (2003) introduced the idea of moving kriging interpolation (MK) and show how it can be used to formulate a new type of meshless method in heat conduction problems. Long and Atluri (2002) extended the meshless local Petrov–Galerkin (MLPG) method for solving thin plate bending problems. Li et al. (2005) utilized the kinematics of a three-dimensional solid of the conventional plate assumption, and proposed a lock-free MLPG formulation for plates. Sladek et al. (2002a,b) decomposed the biharmonic differential equation into Poisson equations, and derived the local boundary integral equations (LBIE) for the thin plate bending problems. Leitao (2001) and Bitaraf and Mohammadi (2010) combined the point interpolation technique with the collocation scheme to derive system of governing equations, and proposed the finite point method (FPM). Based on the recursive composite multiple reciprocity method, Fu and Chen (2009) and Fu et al. (2009) employed a boundary-only collocation scheme-boundary particle method (BPM) to simulate the bending problems of the Kirchhoff plate and Winkler plate. All of these meshless methods do not need an element mesh for the interpolation of the field or boundary variables; however, some of them require background cells for numerical integration, which makes these methods being not "truly" meshless method. Recently, Sladek et al. (2013) applied the new field variable for solving thin plate bending problems by meshless method comparing the solution using either the moving least squares (MLS) approximation or point interpolation approximation. Liu and Huang (2013) used integral identities in order to develop weakly-singular and non-singular forms of the BIEs for plate bending problems. In 2011, Chen et al. (2011) proposed a solution procedure based on the meshless local Petrov–Galerkin (MLPG) method for lower-bound shakedown analysis of bounded kinematic hardening structures. The natural neighbour interpolation (NNI) was employed to construct trial functions for simplifying the imposition of essential boundary conditions. The kinematic hardening behavior was simulated by an overlay model and the numerical difficulties caused by the time parameter were overcome by introducing the conception of load corner. The reduced-basis technique was applied to solve the mathematical programming iteratively through a sequence of reduced residual stress subspaces with very low dimensions and the resulting non-linear programming sub-problems were solved via the Complex method. In 2011, Chen et al. (2011) developed the meshless local natural neighbor interpolation (MLNNI) method to perform the dynamic analysis of elastoplastic structures under plane stress or plane strain conditions. The MLNNI, as an effective truly meshless method for solving partial differential equations, employs local weak forms over a local subdomain and shape functions from the natural neighbor interpolation (NNI). The shape functions so formulated possess delta function property and, therefore, the essential boundary conditions can be implemented as easily as in the finite element method (FEM). The predictor–corrector form of the Newmark algorithm is used for the time-marching process and iterations are performed at every time step. In 2013, Li et al. (2013) developed a numerical meshless model for analyzing transient heat conductions in three-dimensional (3D) axisymmetric continuously non-homogeneous functionally graded materials (FGMs). Axial symmetry of geometry and boundary conditions reduced the original 3D initial-boundary value problem into a two-dimensional (2D) problem. Local weak forms were derived for small polygonal sub-domains which surrounded nodal points distributed over the cross section. In order to simplify the treatment of the essential boundary conditions, spatial variations of the temperature and heat flux at discrete time instants were interpolated by the natural neighbor interpolation. Moreover, the using of three-node triangular finite element method (FEM) shape functions as test functions reduced the orders of integrands involved in domain integrals. The semi-discrete heat conduction equation was solved numerically with the traditional two-point difference technique in the time domain.

The purpose of this paper is to present the meshless method with two field variables local weak form for solving thin simply supported plate problems subjected to various loads. In the present method, the moving kriging (MK) interpolation method using regular and irregular nodal arrangements is employed to construct the nodal shape function as well as the Heaviside step function is used as the test function. In order to verify the validity of this approach, selected numerical examples are analyzed comparing with exact solutions to demonstrate the convergence of the present method which is implemented by maximum relative error and root mean square relative error.

2. Moving kriging interpolation shape function

Similar to the MLS approximation, the moving kriging (MK) method, see (Yimnak and Luadsong, 2014), can be extended to any sub-domain $\Omega_x \subseteq \Omega$. Generally, the MK interpolation $\widetilde{w}(\mathbf{x})$ is defined by Liu (2003)

$$\widetilde{w}(\mathbf{x}) = \sum_{i=1}^{N} \phi_i(x)\hat{w}_i = \Phi(\mathbf{x})\widehat{\mathbf{W}}, \quad \forall \mathbf{x} \in \Omega_x \tag{1}$$

and the shape function $\Phi(\mathbf{x})$ is defined by

$$\Phi(\mathbf{x}) = \mathbf{p}^{\mathrm{T}}(\mathbf{x})\mathbf{A} + \mathbf{r}^{\mathrm{T}}(\mathbf{x})\mathbf{B}, \tag{2}$$

where $\mathbf{p}^{\mathrm{T}}(\mathbf{x}) = [\,p_1(\mathbf{x}) \quad p_2(\mathbf{x}) \quad \ldots \quad p_m(\mathbf{x})\,]$ is a complete monomial basis and $\widehat{\mathbf{W}} = [\,\widehat{w}(\mathbf{x}_1) \quad \widehat{w}(\mathbf{x}_2) \quad \ldots \quad \widehat{w}(\mathbf{x}_N)\,]$.

Introduce the notation

$$\mathbf{A} = (\mathbf{P}^{\mathrm{T}}\mathbf{R}^{-1}\mathbf{P})^{-1}\mathbf{P}^{\mathrm{T}}\mathbf{R}^{-1}, \tag{3}$$

$$\mathbf{B} = \mathbf{R}^{-1}(\mathbf{I} - \mathbf{P}\mathbf{A}). \tag{4}$$

The matrices $\mathbf{P}, \mathbf{R}$ and vector $\mathbf{r}^{\mathrm{T}}(\mathbf{x})$ are given as follows:

$$\mathbf{P} = \begin{bmatrix} p_1(\mathbf{x_1}) & p_2(\mathbf{x_1}) & \ldots & p_m(\mathbf{x_1}) \\ p_1(\mathbf{x_2}) & p_2(\mathbf{x_2}) & \ldots & p_m(\mathbf{x_2}) \\ \vdots & \vdots & \ddots & \vdots \\ p_1(\mathbf{x_N}) & p_2(\mathbf{x_N}) & \ldots & p_m(\mathbf{x_N}) \end{bmatrix}, \tag{5}$$

$$\mathbf{R} = \begin{bmatrix} \gamma(\mathbf{x_1}, \mathbf{x_1}) & \gamma(\mathbf{x_1}, \mathbf{x_2}) & \ldots & \gamma(\mathbf{x_1}, \mathbf{x_N}) \\ \gamma(\mathbf{x_2}, \mathbf{x_1}) & \gamma(\mathbf{x_2}, \mathbf{x_2}) & \ldots & \gamma(\mathbf{x_2}, \mathbf{x_N}) \\ \vdots & \vdots & \ddots & \vdots \\ \gamma(\mathbf{x_N}, \mathbf{x_1}) & \gamma(\mathbf{x_N}, x_2) & \ldots & \gamma(\mathbf{x_N}, \mathbf{x}_N) \end{bmatrix}, \tag{6}$$

$$\mathbf{r}^{\mathrm{T}}(\mathbf{x}) = [\,\gamma(\mathbf{x}, \mathbf{x_1}) \quad \gamma(\mathbf{x}, \mathbf{x_2}) \quad \ldots \gamma(\mathbf{x}, \mathbf{x_N})\,], \tag{7}$$

and $\mathbf{I}$ is an $n \times n$ identity matrix.

The $\gamma(\mathbf{x_i}, \mathbf{x}_j)$ is the dimensionless correlation Gaussian function between any pair of nodal points located at $\mathbf{x_i}$ and $\mathbf{x_j}$, namely

$$\gamma(\mathbf{x_i}, x_j) = e^{-\theta\left(\frac{r_{ij}}{d_c}\right)^2}, \tag{8}$$

where $r_{ij} = \|\mathbf{x_i} - \mathbf{x_j}\|$, $\theta > 0$ is the dimensionless shape parameter and d_c is a characteristic length that is related to the nodal spacing in the local domain of the point of interest.

Literally, Eq. (2) can also be rewritten as

$$\widetilde{w}(\mathbf{x}) = \left[\mathbf{p}^{\mathrm{T}}(\mathbf{x})\mathbf{A} + \mathbf{r}^{\mathrm{T}}(\mathbf{x})\mathbf{B}\right]\widehat{\mathbf{W}}, \tag{9}$$

where the shape function and its first derivative can be defined as follows:

$$\phi_i(\mathbf{x}) = \sum_{j=1}^{m} p_j(\mathbf{x})\mathbf{A}_{ji} + \sum_{k=1}^{n} r_k(\mathbf{x})\mathbf{B}_{ki}, \tag{10}$$

$$\phi_{i,l}(\mathbf{x}) = \sum_{j=1}^{m} p_{j,l}(\mathbf{x})\mathbf{A}_{ji} + \sum_{k=1}^{n} r_{k,l}(\mathbf{x})\mathbf{B}_{ki}. \tag{11}$$

The index following a comma is a spatial derivative.

3. Governing equations and discretization

In the classical Kirchhoff's theory of bending of thin plates (Timoshenko and Woinowsky-Krieger, 1959), the governing equation which results in the biharmonic equation may be written as

$$\nabla^4 w(\mathbf{x}) = \frac{q(\mathbf{x})}{D} \quad \mathbf{x} \in \Omega, \tag{12}$$

where $w(\mathbf{x})$ is the plate deflection, $q(\mathbf{x})$ is the prescribed load normal to the plate, $\nabla^4(\cdot)$ is a biharmonic operator, and D is the flexural rigidity being given as $D = \frac{Eh^3}{12(1-\nu^2)}$ where E is the Young's modulus, ν is the Poisson ratio, and h is the plate thickness.

The plate domain $\Omega = [0,1] \times [0,1]$ is enclosed by the following simply supported boundary conditions edge Γ:

$$\begin{aligned}
&w(0,y) = 0; \qquad w(1,y) = 0,\\
&w(x,0) = 0; \qquad w(x,1) = 0,\\
&\frac{\partial^2 w(0,y)}{\partial x^2} = 0; \qquad \frac{\partial^2 w(1,y)}{\partial x^2} = 0,\\
&\frac{\partial^2 w(x,0)}{\partial y^2} = 0; \qquad \frac{\partial^2 w(x,1)}{\partial y^2} = 0.
\end{aligned} \tag{13}$$

Introducing the new field variable and assuming the flexural rigidity to be constant, we obtain

$$m(\mathbf{x}) := -\nabla^2 w(\mathbf{x}), \tag{14}$$

$$\nabla^2 m(\mathbf{x}) = -\frac{q(\mathbf{x})}{D}. \tag{15}$$

Using the local weighted residual method, Eqs. (14) and (15) become

$$\int_{\Omega_s^i} \left(\nabla^2 w + m\right) v_i d\Omega = 0, \tag{16}$$

and

$$\int_{\Omega_s^i} \left(\nabla^2 m + \frac{q}{D}\right) v_i d\Omega = 0, \tag{17}$$

where v_i is the test function.

Using the Heaviside unit step function as the test function and applying the Green's first identity in Eqs. (16) and (17), the following local weak forms can be obtained

$$\int_{\partial\Omega_s^i} \frac{\partial w}{\partial \mathbf{n}} d\Gamma + \int_{\Omega_s^i} m d\Omega = 0, \tag{18}$$

and

$$\int_{\partial\Omega_s^i} \frac{\partial m}{\partial \mathbf{n}} d\Gamma + \int_{\Omega_s^i} \frac{q}{D} d\Omega = 0, \tag{19}$$

where $\mathbf{n}$ is the cartesian component of the outward unit normal vector on boundary edges. Next, transverse deflection w and new variable m are interpolated using MK as

$$\widetilde{w}(\mathbf{x}) \approx \sum_{j=1}^{N} \phi_j \widehat{w}_j, \tag{20}$$

$$\widetilde{m}(\mathbf{x}) \approx \sum_{j=1}^{N} \phi_j \widehat{m}_j. \tag{21}$$

Substituting the these expressions into local weak form Eqs. (18) and (19), the discrete equation for each node is obtained as follows:

$$\begin{bmatrix} \int_{\partial\Omega_s^i} \frac{\partial \phi_j(\mathbf{x}_i)}{\partial \mathbf{n}} d\Gamma & \int_{\Omega_s^i} \phi_j(\mathbf{x}_i) d\Omega \\ 0 & \int_{\partial\Omega_s^i} \frac{\partial \phi_j(\mathbf{x}_i)}{\partial \mathbf{n}} d\Gamma \end{bmatrix} \begin{bmatrix} \widehat{w}_1 \\ \vdots \\ \widehat{w}_N \\ \widehat{m}_1 \\ \vdots \\ \widehat{m}_N \end{bmatrix} = \begin{bmatrix} 0 \\ -\int_{\Omega_s^i} \frac{q}{D} d\Omega \end{bmatrix}, \tag{22}$$

where $i, j = 1, 2, \ldots, N$.

4. Numerical examples

In this section, some numerical results are presented to verify our approach by comparing with an exact solution. The accuracy is illustrated by plotting the selected number of nodal points versus the maximum relative error as well as root mean square relative error in tests of accuracy of approximation for deflections at evaluation. Both the errors are defined as

$$\varepsilon_{max} = \max \left| \frac{\widetilde{w} - w^{ex}}{w^{ex}} \right|, \tag{23}$$

$$\varepsilon_{rms} = \sqrt{\frac{1}{N} \sum_{k=1}^{N} \left(\frac{\widetilde{w}(\mathbf{x}_k) - w^{ex}(\mathbf{x}_k)}{w^{ex}(\mathbf{x}_k)} \right)^2}. \tag{24}$$

Linear and quadratic polynomial bases are chosen at first in order to construct nodal shape function. Correlation parameter is set as 0.5 for being a smooth curve while the radius of each local sub-domain should be big enough such that the union of all local sub-domains covers as much as possible in order to avoid singularity of calculated matrices. For this reason, the radius of the local sub-domain of each boundary node is taken as 0.7 times minimum nodal points while 21 gaussian points are used on each section of Γ. Regular and irregular nodal distribution are chosen as $16(4 \times 4)$, $25(5 \times 5)$,

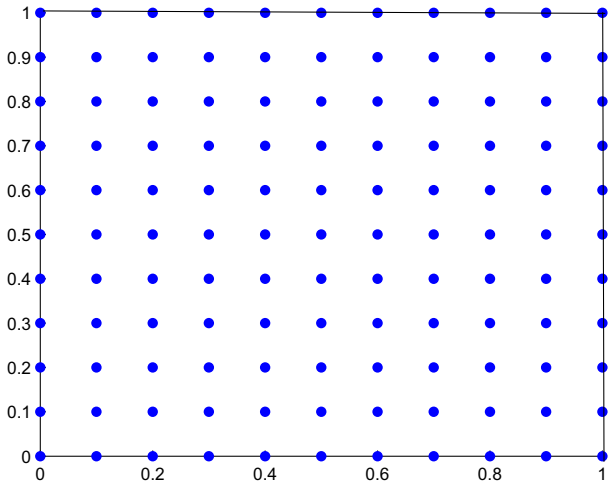

Figure 1 Nodal distribution in the square plate with 11×11 regular scattered nodes.

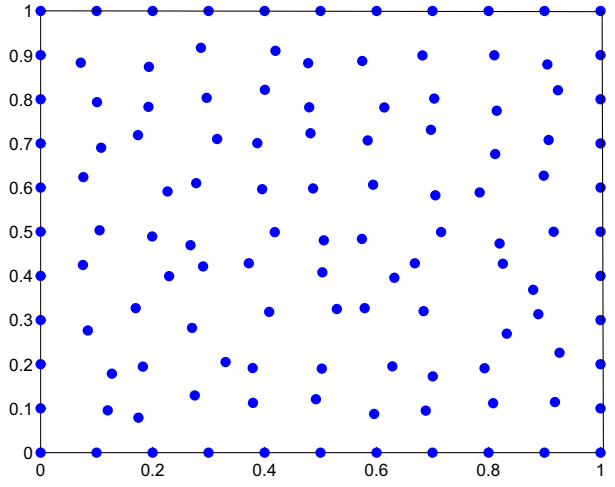

Figure 2 Nodal distribution in the square plate with 121 irregular scattered nodes.

$36(6 \times 6)$, $49(7 \times 7)$, $64(8 \times 8)$, $81(9 \times 9)$, $100(10 \times 10)$ and $121(11 \times 11)$. Illustratively, nodal distribution in the square plate with 11×11 regular and 121 irregular scattered nodes are shown in Figs. 1 and 2, respectively.

For numerical implementation, selected a simply supported rectangular plate under sinusoidal load, uniformly distributed load, hydrostatic load and a hollow plate are implemented as follow:

4.1. Sinusoidal load on a simply supported rectangular plate

An exact solution in term of deflection is given by Timoshenko and Woinowsky-Krieger (1959).

$$w(x,y) = \frac{q_0}{\pi^4 D\left(\frac{1}{a^2}+\frac{1}{b^2}\right)^2} \sin\frac{\pi x}{a} \sin\frac{\pi y}{b}, \tag{25}$$

where $q(x,y) = q_0 \sin\frac{\pi x}{a} \sin\frac{\pi y}{b}$, $q_0 =$ represents the intensity of the load at the center of the plate, D is the flexural rigidity, and a, b are the side lengths of a rectangular plate.

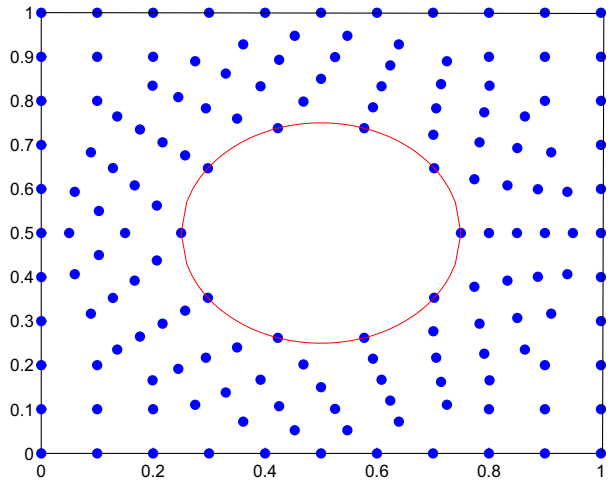

Figure 3 Nodal distribution in the hollow plate with 152 irregular scattered nodes.

For both the errors caused by introducing two-filed variables of this method, tabular errors using linear basis for selected number of nodal points of Example 4.1 are shown in Table 1 while Table 2 shows the errors using quadratic basis instead. According to both tables, these results show the convergence of this method by increasing the number of nodal points which can be see as an increasing accuracy by increasing the number of nodal points. In addition, illustratively, the fictitious values w versus exact solution and absolute value of the difference between exact solution and approximate solutionis are shown in Fig. 4 while the results of absolute maximum relative errors and root mean square relative errors are shown in Figs. 5 and 6, respectively.

4.2. Uniformly distributed load on a simply supported rectangular plate

An exact solution in term of deflection is given by Timoshenko and Woinowsky-Krieger (1959)

$$w(x,y) = \frac{16q}{\pi^6 D} \sum_m \sum_n \frac{1}{mn\left(\frac{m^2}{a^2}+\frac{n^2}{b^2}\right)^2} \times \sin\frac{m\pi x}{a} \sin\frac{n\pi y}{b}, \quad m,\ n = 1,\ 3,\ 5,\ \ldots, \tag{26}$$

where $q(x,y) = q$, q represents a uniformly distributed load, D is the flexural rigidity, and a, b are the side lengths of a rectangular plate.

Table 1 Maximum relative errors and root mean square of relative errors using linear basis for nodal construction of Example 4.1.

n	ε_{max}	ε_{rms}
16	0.087161168170710	0.043580584085307
25	0.050358497618669	0.030113754701725
36	0.032361053913413	0.021484740518138
49	0.023035676208513	0.016387047401505
64	0.017143934984936	0.012673300080537
81	0.013492037450895	0.010323479185026
100	0.010879139865142	0.008417391483891
121	0.002336287440439	0.001632271994812

Table 2 Maximum relative errors and root mean square of relative errors using quadratic basis for nodal construction of Example 4.1.

n	ε_{max}	ε_{rms}
16	0.091657933473486	0.045828966736731
25	0.050623969866327	0.030352930169516
36	0.031908920567838	0.021037079186475
49	0.022606591744903	0.015987485213218
64	0.016482360093915	0.012121872348316
81	0.012806666014302	0.009807325440163
100	0.010070455041601	0.007871532231840
121	0.001516655001101	0.001107414913633

Likewise, for both of errors caused by introducing two-filed variables of this method, tabular errors using linear basis for selected number of nodal points of Example 4.2 are shown in Table 3 while Table 4 are shown the errors using quadratic basis instead. According to both tables, These results show the convergence of this method by increasing the number of nodal points which can be see as increasing accuracy by increasing the number of nodal points. In addition, illustratively, the fictitious values w versus exact solution and absolute value of the difference between exact solution and approximate solutionis are shown in Fig. 7 while the results of absolute maximum relative errors and root mean square relative errors are shown in Figs. 8 and 9, respectively.

4.3. Hydrostatic load on a simply supported rectangular plate

An exact solution in terms of deflection is given by Rudolph (1974)

$$w(x,y) = \frac{8q}{\pi^6 D}\sum_{m=}\sum_{n}\frac{(-1)^{m+1}}{mn\left(\frac{m^2}{a^2}+\frac{n^2}{b^2}\right)^2} \times \sin\frac{m\pi x}{a}\sin\frac{n\pi y}{b}, \quad m,\ n = 1,\ 2,\ 3,\ \ldots, \tag{27}$$

where $q(x,y) = \frac{qx}{a}$ is a hydrostatic load, q represents a uniformly distributed load, D is the flexural rigidity, and a, b are the side lengths of a rectangular plate. Irregular nodal arrangement shown in Fig. 2 is conducted for constructing shape function . Illustratively, the fictitious values w and exact solution

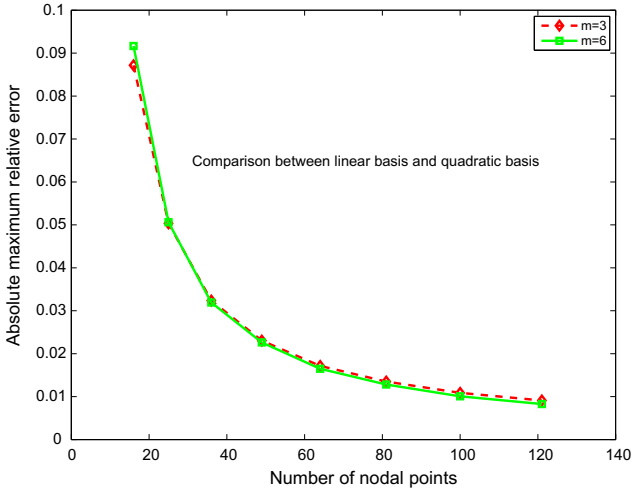

Figure 5 Maximum relative errors as a function of nodal points of Example 4.1.

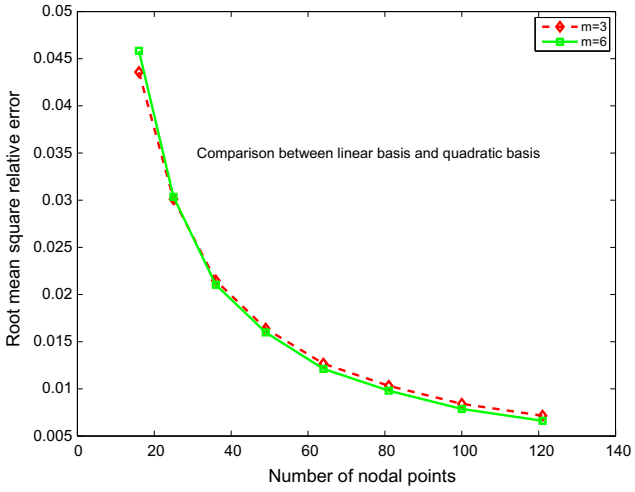

Figure 6 Root mean square relative errors as a function of nodal points of Example 4.1.

corresponding linear and quadratic polynomial basis are shown in Figs. 10 and 11, respectively.

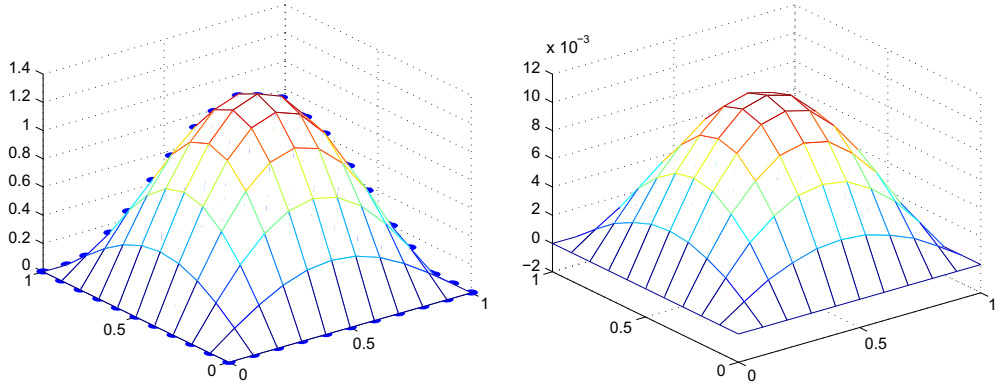

Figure 4 Exact solution versus fictitious values (left) and absolute value of the difference between exact solution and approximate solution (right) of Example 4.1, 11×11 regular nodal distribution with linear polynomial basis.

Table 3 Maximum relative errors and root mean square of relative errors using linear basis for nodal construction of Example 4.2.

n	ε_{max}	ε_{rms}
16	0.009380370258943	0.004690185129419
25	0.010227433424274	0.004485160943519
36	0.009239014511950	0.003682568495845
49	0.008370612949564	0.003184019437063
64	0.006690798478377	0.002493855584604
81	0.005456953335600	0.002188658062610
100	0.003647844775999	0.001742330978038
121	0.002669141979986	0.001031499111947

Table 4 Maximum relative errors and root mean square of relative errors using quadratic basis for nodal construction of Example 4.2.

n	ε_{max}	ε_{rms}
16	0.014260294100857	0.007130147050416
25	0.014090587400685	0.006303146486460
36	0.009092940658449	0.003601777152419
49	0.008382851789990	0.003165358484080
64	0.005693541722870	0.002058154266352
81	0.004422561209010	0.001764431690954
100	0.002573194839596	0.001215442051533
121	0.001853860804109	0.000639748726227

4.4. A simply supported hollow plate

An exact solution in term of deflection is given by

$$w(x,y) = \left(\left(x-\frac{1}{2}\right)^2 + \left(y-\frac{1}{2}\right)^2 - \left(\frac{1}{5}\right)^2\right)^3 \sin(\pi x)\sin(\pi y). \tag{28}$$

For Problem 4.4, nodal distribution in the hollow plate with 152 irregular scattered nodes is shown in Fig. 3. Apparently, using linear basis and quadratic basis, an approximate solution profile gives a significant outcome that is as same as an exact solution profile which is illustrated by Figs. 12 and 13,

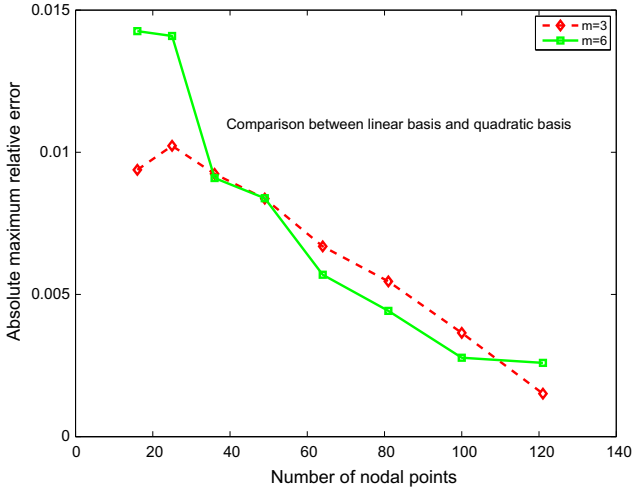

Figure 8 Maximum relative errors as a function of nodal points of Example 4.2.

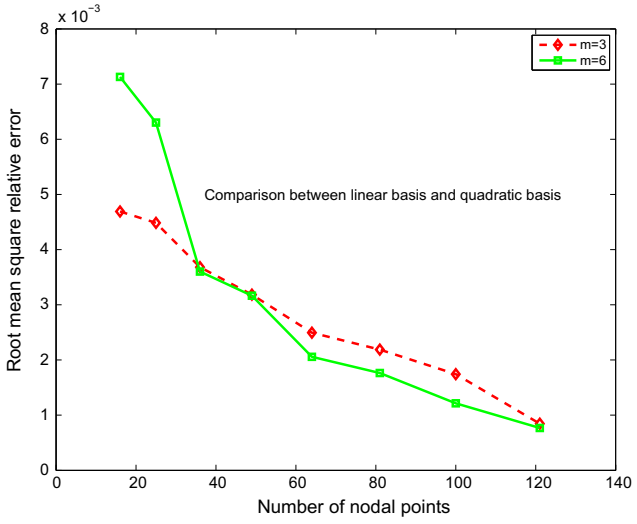

Figure 9 Root mean square relative errors as a function of nodal points of Example 4.2.

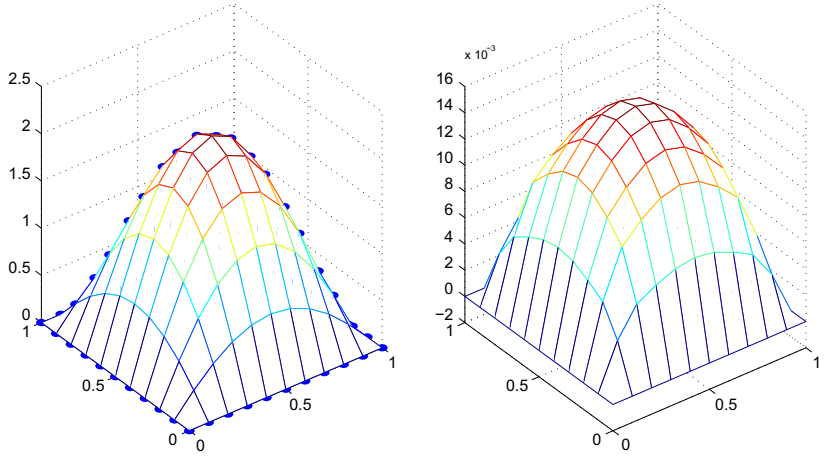

Figure 7 Exact solution versus fictitious values (left) and absolute value of the difference between exact solution and approximate solution (right) of Example 4.3, 11×11 regular nodal distribution with quadratic polynomial basis.

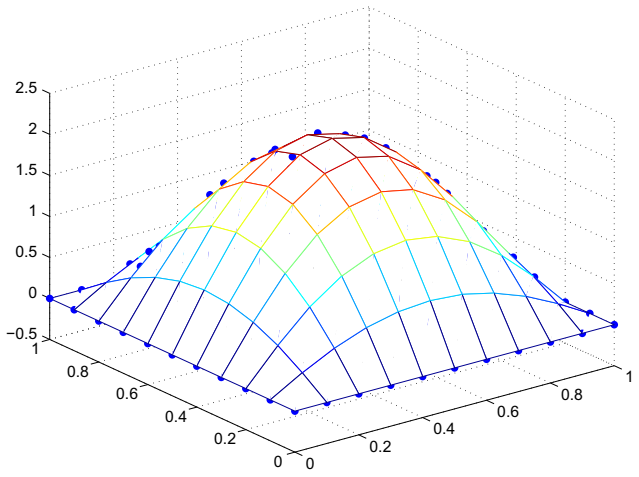

Figure 10 Exact solution versus fictitious values of Example 4.3, 121 irregular nodal distribution with linear polynomial basis.

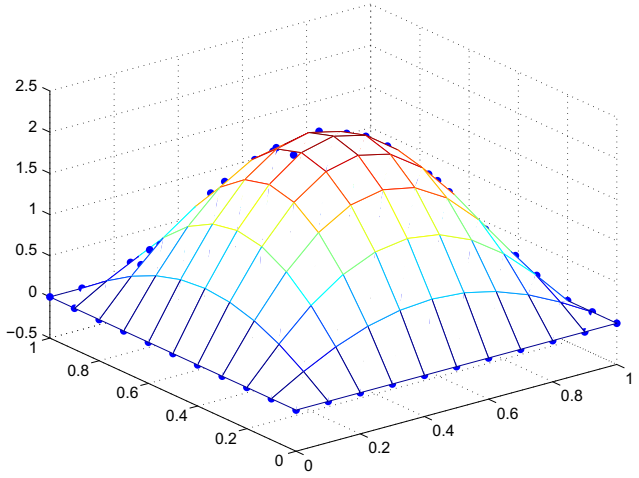

Figure 11 Exact solution versus fictitious values of Example 4.3, 121 irregular nodal distribution with quadratic polynomial basis.

respectively. In addition, the maximum absolute value of the difference between an exact solution and an approximate solution is approximately 0.001376 while the maximum of root mean square value of the difference between an exact solution and an approximate solution is approximately 0.000722 when using both linear polynomial basis and quadratic polynomial basis for constructing nodal shape functions.

According to numerical results, both the errors using quadratic polynomial basis are less than both the errors using linear polynomial basis; moreover, increasing a number of nodal points can be decreased maximum relative errors and root mean square relative errors. Typically, quadratic-polynomial-basis usage is a better criterion constructing the nodal shape function than linear-polynomial-basis usage; furthermore, increasing a number of nodal points can decrease maximum relative errors and root mean square relative errors. Irregular nodal arrangement can also consider constructing shape function. It can be seen that the agreements between numerical and analytical results are quite excellent, and the convergence is very good as well as computational efficiency.

5. Conclusions

An alternative approach of meshless method for solving thin plates is presented in the present work. The moving kriging interpolation method can also be used for constructing nodal shape functions as well as two-field variables scheme and is proposed in order to decompose the biharmonic equation into a coupled of Poisson's equations; furthermore, two-field variable local weak forms using Heaviside step function enable us to simplify the complicated conventional local weak form of the biharmonic equation as well as impose straightforward the simply supported boundary condition, For these reasons, computer literacy is also conducted systematically in the sense of easiness and robustness and its implementation is also acceptable as well. Comparing between exact solution and approximate solution for all examples, numerical results shows that usage of the quadratic polynomial and linear basis can give quite accurate numerical results.

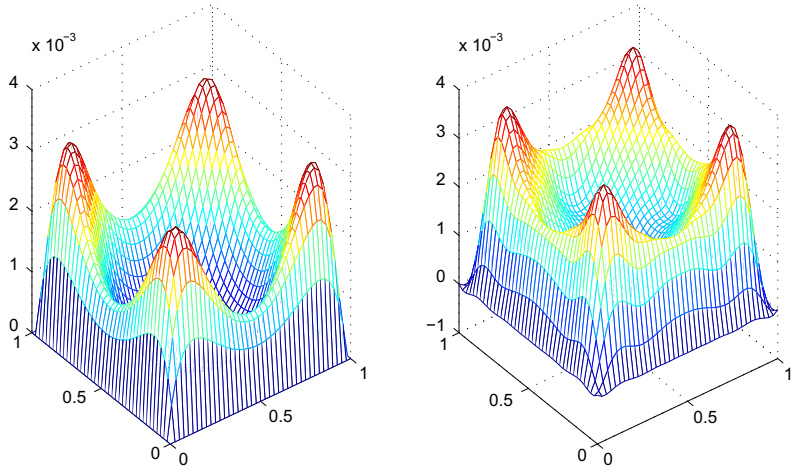

Figure 12 A comparison of an exact solution (left) and an approximate solution (right) of Example 4.4, 152 irregular nodal distribution with linear polynomial basis.

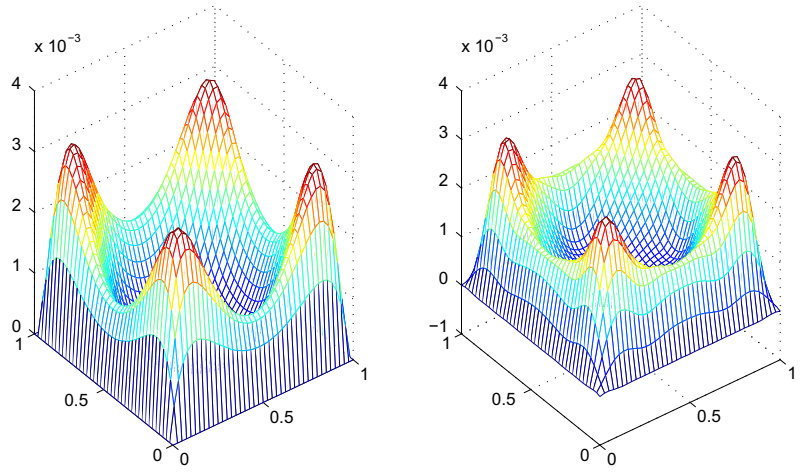

Figure 13 A comparison of an exact solution (left) and an approximate solution (right) of Example 4.4, 152 irregular nodal distribution with quadratic polynomial basis.

Acknowledgments

The authors would like to thank the Department of Mathematics, KMUTT, Thailand, for facilities during this research. Moreover, the authors would like to thank their parents and family, who have also been encouraging, as well as their friends for taking care of each other. Finally, the authors would like to thank the referees for their useful comments and language editing, which greatly improved the manuscript.

References

Bitaraf, M., Mohammadi, S., 2010. Large deflection analysis of flexible plates by the meshless finite point method. Thin Wall. Struct. 48, 200–214.

Chen, S.S., Liu, Y.H., Li, J., Cen, Z.Z., 2011. Performance of the MLPG method for static shakedown analysis for bounded kinematic hardening structures. Eur. J. Mech. A Solids 30, 183–194.

Chen, S.S., Li, Q.H., Liu, Y.H., Xia, J.T., Xue, Z.Q., 2011. Dynamic elastoplastic analysis using the meshless local natural neighbour interpolation method. Int. J. Comput. Methods 8 (3), 463–481.

Fu, Z.J., Chen, W., 2009. A truly boundary-only meshfree method applied to Kirchhoff plate bending problems. Adv. Appl. Math. Mech. 1, 757–763.

Fu, Y.T., Chen, W., Yang, W., 2009. Winkler plate bending problems by a truly boundary-only boundary particle method. Comput. Mech. 44, 341–352.

Krysl, P., Belytschko, T., 1995. Analysis of thin plates by the element-free Galerkin method. Comput. Mech. 17, 26–35.

Leitao, V.M.A., 2001. A meshless method for Kirchhoff plate bending problems. Int. J. Numer. Methods Eng. 52, 1107–1130.

Li, Q., Soric, J., Jarak, T., Atluri, S.N., 2005. A locking-free meshless local Petrov–Galerkin formulation for thick and thin plates. Int. J. Comput. Phys. 208, 116–117.

Li, Q.H., Chen, S.S., Zeng, J.H., 2013. A meshless model for transient heat conduction analyses of 3D axisymmetric functionally graded solids. Chin. Phys. B 22 (12), 120204.

Liu, Gu., 2003. Moving kriging interpolation and element-free Galerkin method. Int. J. Numer. Methods Eng. 56, 1–11.

Liu, Y.J., Huang, S., 2013. Identities for the fundamental solution of thin plate bending problems and the nonuniqueness of the hypersingular BIE solution. Eng. Anal. Bound. Elem. 37, 594–602.

Long, S.Y., Atluri, S.N.A., 2002. meshfree local Petrov–Galerkin method for solving the bending problem of a thin plate. Comput. Model. Eng. Sci. 3, 53–63.

Rudolph, Szilard, 1974. Theory and Analysis of Plates. Prentice-Hall, New Jersey.

Sladek, V., Sladek, J., Mang, H.A., 2002a. Meshless formulations for simply supported and clamped plate problems. Int. J. Numer. Methods Eng. 55, 359–375.

Sladek, V., Sladek, J., Mang, H.A., 2002b. Meshless local boundary integral equation method for simply supported and clamped plates resting on elastic foundation. Comput. Methods Appl. Mech. Eng. 191, 5943–5959.

Sladek, V., Sladek, J., Sator, L., 2013. Physical decomposition of thin plate bending problems and their by mesh-free methods. Eng. Anal. Bound. Elem. 37, 348–365.

Timoshenko, S.P., Woinowsky-Krieger, S., 1959. Theory of Plates and Shells. McGraw-Hill, New York.

Yimnak, K., Luadsong, A., 2014. A local integral equation formulation based on moving kriging interpolation for solving coupled nonlinear reaction–diffusion equations. Adv. Math. Phys. 2014 (7). http://dx.doi.org/10.1155/2014/196041. Article ID 196041.